Phase diagrams of $\mathrm{Ba(Fe_{1-x}TM_x)_2As_2}$ (TM = Rh, Pd) single crystals

N. Ni, A. Thaler, A. Kracher, J. Q. Yan, S. L. Bud'ko, and P. C. Canfield

Ames Laboratory and Department of Physics and Astronomy,

Iowa State University, Ames, IA 50011, USA

(Dated: May 29, 2009)

Abstract

Single crystalline $\mathrm{Ba(Fe_{1-x}TM_x)_2As_2}$ (TM = Rh, Pd) series have been grown and characterized by structural, thermodynamic and transport measurements. These measurements show that the structural/magnetic phase transitions, found in pure $\mathrm{BaFe_2As_2}$ at 134 K, are suppressed monotonically by the doping and that superconductivity can be stablized over a dome-like region. Temperature-composition $(T - x)$ phase diagrams based on electrical transport and magnetization measurements are constructed and compared to those of the $\mathrm{Ba(Fe_{1-x}TM_x)_2As_2}$ (TM = Co, Ni) series. Despite the generic difference between $3d$ and $4d$ shells and the specific, conspicuous differences in the changes to the unit cell parameters, the effects of Rh doping are exceptionally similar to the effects of Co doping and the effects of Pd doping are exceptionally similar to the effects of Ni doping. These data show that whereas the structural / antiferromagnetic phase transition temperatures can be parameterized by x and the superconducting transition temperature can be parameterized by some combination of x and e, the number of extra electrons associated with the TM doping, the transition temperatures of $3d-$ and $4d-$ doped $\mathrm{BaFe_2As_2}$ can not be simply parameterized by the changes in the unit cell dimensions or their ratios.

PACS numbers: 74.10.+v; 74.62.Dh; 74.70.Dd; 75.30.Kz

I. INTRODUCTION

The discovery of superconductivity in F-doped LaFeAsO [1] and K-doped BaFe$_2$As$_2$ [2] compounds in the first half of 2008 has led to extensive experimental interest; T_c has risen as high as 56 K for F doped RFeAsO systems [3] and as high as 38 K in K and Na doped (AE)Fe$_2$As$_2$ systems (AE: Ba, Sr, Ca) [2]. Soon after, superconductivity was also found in Co and Ni doped (AE)Fe$_2$As$_2$ [4, 5] and RFeAsO [6]. Recently, superconductivity was also found in $4d$ and $5d$ transition metal electron doped SrFe$_2$As$_2$ [7, 8, 9, 10]. Although electron doped (AE)Fe$_2$As$_2$ systems have lower T_c values ($\sim$24 K) [11, 12, 13, 14], intensive studies have been made on them because doping is more homogeneous in these systems and the single crystals can be easily grown and reproduced. For example, several studies of Ba(Fe$_{1-x}$Co$_x$)$_2$As$_2$ system have resulted in remarkably similar data and conclusions [11, 12, 13, 14]. In order to compare the effects of $3d$ and $4d$ electron doping in BaFe$_2$As$_2$, and thus try to understand the conditions for the appearance of superconductivity in these systems, carefully constructed $T-x$ phase diagrams are needed. Elemental analysis, preferably of single crystal samples, should be used to determine the actual percentage of the dopant inside the lattice rather than the nominal doping level. Recently such a detailed study was made for Co doped BaFe$_2$As$_2$ [11, 12, 13, 14, 15, 16], as well as for Ni, Cu, and Cu/Co mixes [17]. These data on $3d$, electron doped BaFe$_2$As$_2$ raised the question of whether the number of impurities, the band filling, and / or the unit cell dimensions were the physically salient variables. For this paper, Ba(Fe$_{1-x}$TM$_x$)$_2$As$_2$ (TM = Rh, Pd) series have been studied by the electrical transport, magnetization, specific heat and wave-length dispersive spectroscopy. We find that the $T-x$ phase diagrams for Co- and Rh-doping are virtually identical, as are the phase diagrams for Ni- and Pd-doping. By analysis of the relative changes in the unit cell parameters we can conclude that whereas x and e can still successfully be used to parameterize the structual / magentic and superconducting phase transitions in the Ba(Fe$_{1-x}$TM$_x$)$_2$As$_2$ systems, changes in the unit cell parameters, or their ratios, no longer can.

II. EXPERIMENTAL METHODS

Single crystals of Ba(Fe$_{1-x}$TM$_x$)$_2$As$_2$(TM = Rh, Pd) were grown out of self flux using conventional high-temperature solution growth techniques [11, 17, 18]. FeAs, RhAs and

PdAs powder were synthesized in the same manner as in [11]. Small Ba chunks, FeAs/RhAs or FeAs/PdAs powder were mixed together according to the ratio Ba:TMAs = 1:4. The mixture was placed into an alumina crucible with a second "catch" crucible containing quartz wool placed on top. Both crucibles were sealed in a quartz tube under a 1/3, partial atmosphere, of Ar gas. The sealed quartz tube was heated up to 1180 °C over 12 hours, held at 1180 °C for 5 hours, and then cooled to 1050 °C over 36 hours. Once the furnace reached 1050 °C, the excess FeAs/RhAs or FeAs/PdAs liquid was decanted from the plate like single crystals.

Powder x-ray diffraction measurements, with a Si standard, were performed using a Rigaku Miniflex diffractometer with Cu K_α radiation at room temperature. Diffraction patterns were taken on ground single crystals from each batch. No detectable impurities were found in these compounds. The unit cell parameters were refined by "UnitCell" software. Error bars were taken as twice the standard deviation, σ, which was obtained from the refinements by the "Unitcell" software. Elemental analysis of the samples was performed using wavelength dispersive x-ray spectroscopy (WDS) in the electron probe microanalyzer of a JEOL JXA-8200 electron-microprobe. Magnetization and temperature-dependent AC electrical resistance data (f=16Hz, I=3mA) were collected in a Quantum Design (QD) Magnetic Properties Measurement System (MPMS) using LR700 resistance bridge for the latter. Electrical contact was made to the sample using Epotek H20E silver epoxy to attach Pt wires in a four-probe configuration. Heat capacity data were collected using a QD Physical Properties Measurement System (PPMS) using the relaxation technique.

III. RESULTS

Summaries of the WDS measurement data are shown in Table I for both $Ba(Fe_{1-x}Rh_x)_2As_2$ and $Ba(Fe_{1-x}Pd_x)_2As_2$. For each batch, up to 5 pieces of samples were measured. The table shows the number of locations measured, the average of the x values measured at these locations, and two times the standard deviation of the x values measured on these locations, which is taken as the error bar in this paper. We can see that the 2σ error bars are $\lesssim 10\%$ of the average x values. The average x value, x_{ave}, obtained from wavelength dispersive x-ray spectroscopy (WDS) measurement will be used for all the compounds in this paper rather than nominal x. It is worth noting that separate measurements of x_{ave} on

3

the resistivity bars gave values within the 2σ error bars for all the measured batches.

$Ba(Fe_{1-x}Rh_x)_2As_2$							
N	16	16	18	15	20	34	33	20
x_{ave}	0.012	0.026	0.039	0.057	0.076	0.096	0.131	0.171
2σ	0.001	0.001	0.002	0.003	0.004	0.006	0.005	0.002
$Ba(Fe_{1-x}Pd_x)_2As_2$							
N	18	8	52	6	6	12	14	52
x_{ave}	0.012	0.021	0.027	0.030	0.043	0.053	0.067	0.077
2σ	0.001	0.002	0.003	0.002	0.001	0.002	0.002	0.005

TABLE I: The WDS data for $Ba(Fe_{1-x}Rh_x)_2As_2$ and $Ba(Fe_{1-x}Pd_x)_2As_2$. N is the number of locations measured in one batch, x_{ave} is the average x value measured in one batch, 2σ is two times the standard deviation of the N values measured.

Fig. 1 presents the normalized electrical resistivity data of the $Ba(Fe_{1-x}Rh_x)_2As_2$ series from base temperature, 2 K, to 300 K. Normalized resistivity, instead of resistivity, is plotted because of the tendancy of these samples to exfoliate or partially crack [11, 19, 20]. The resistive anomaly at 134 K for pure $BaFe_2As_2$ is associated with the structural/magnetic phase transitions [21]. As in the case of Co, Ni and Cu substitutions [11, 17], as x is increased the temperature of the resistive anomaly is suppressed monotonically and the shape of the feature changes from a sharp decrease in pure $BaFe_2As_2$ to a broadened increase in doped samples. It is no longer detectable for $x \geq 0.057$. For $x = 0.026$, superconductivity becomes detectable, with $T_c \approx 3$ K inferred from the sharp drop in the resistivity data. For $x = 0.057$, superconducting temperature T_c has a maximum value of 24 K with a width $\Delta T_c \approx 0.7$ K. With even higher x, T_c is suppressed.

Fig. 2 shows the M/H data for the $Ba(Fe_{1-x}Rh_x)_2As_2$ series taken at 25 Oe with H perpendicular to the crystallographic c-axis. A clear diamagnetic signal can be seen in both field-cooled(FC) and zero-field-cooled(ZFC) data. Because of the low T_c values for $x = 0.026$ and $x = 0.131$, which are on the low- and high- x extremes of the superconductivity dome respectively, we only observe the onset of the diamagnetic signal and no large drop below the superconducting temperature is seen down to our base temperature of 2 K. However, for all the other concentrations, the large superconducting, shielding fraction and the sharp
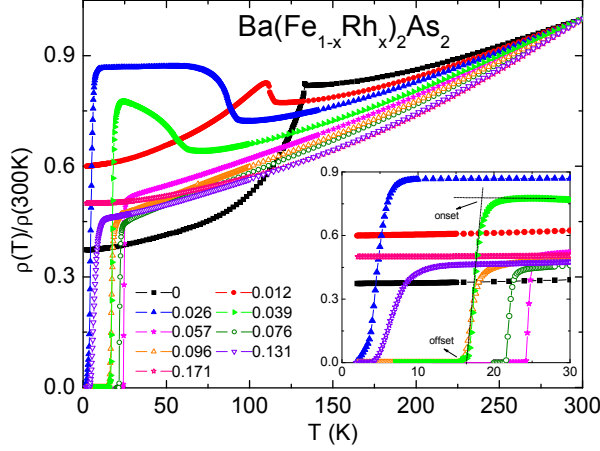
FIG. 1: The temperature dependent resistivity, normalized by the room temperature value, for Ba(Fe$_{1-x}$Rh$_x$)$_2$As$_2$. Inset: low temperature data for Ba(Fe$_{1-x}$Rh$_x$)$_2$As$_2$. Onset and offset criteria for T_c are shown.

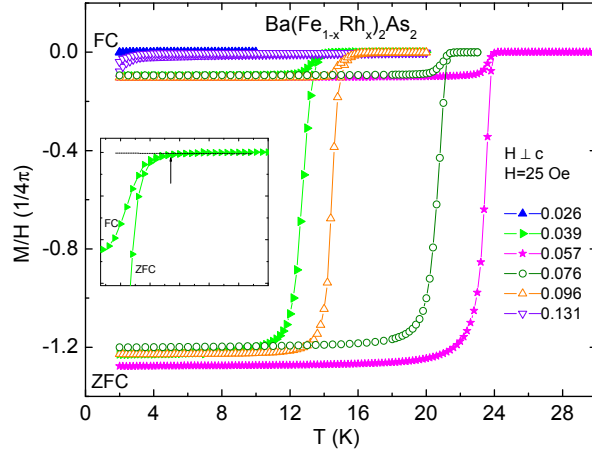FIG. 2: Low magnetic field M/H for Ba(Fe$_{1-x}$Rh$_x$)$_2$As$_2$ series. Inset: The criterion used to infer T_c is shown for Ba(Fe$_{0.961}$Rh$_{0.039}$)$_2$As$_2$.

drop below T_c are consistent with the existence of bulk superconductivity. Compared to the low field M/H data for Ba(Fe$_{1-x}$Co$_x$)$_2$As$_2$ [11], the superconducting fraction associated with the Ba(Fe$_{1-x}$Rh$_x$)$_2$As$_2$ series have very similar values as of Ba(Fe$_{1-x}$Co$_x$)$_2$As$_2$ series.

The temperature dependent heat capacity data for Ba(Fe$_{0.943}$Rh$_{0.057}$)$_2$As$_2$ is shown in Fig. 3. This concentration has the maximum T_c value in this series. The heat capacity anomaly is relatively sharp and consistent with the superconducting phase transition we observed in both resistivity and low field magnetization data. The large arrow in the inset

5

shows the onset of superconductivity and $T_c = 23.2$ K. A way to estimate $\triangle C_p$ is also shown in the inset; $\triangle C_p \approx 700$ mJ/mole K. Assuming the BCS weak coupling approximation $\triangle C_p / \gamma T_c = 1.43$ and 100% superconducting volume, the γ value for $Ba(Fe_{0.943}Rh_{0.057})_2As_2$ can be estimated to be about 20 mJ/mole K^2, which is comparable to the value estimated in the same manner for $Ba(Fe_{0.943}Co_{0.074})_2As_2$ [22].
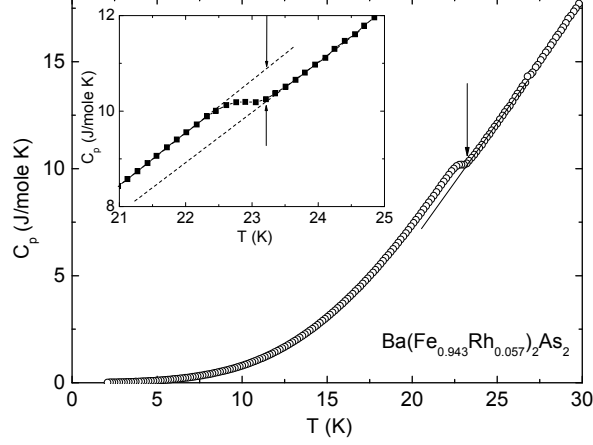

FIG. 3: Temperature dependent heat capacity data for $Ba(Fe_{0.943}Rh_{0.057})_2As_2$. Inset: C_p vs. T near the superconducting transition with the estimated $\triangle C_p$ shown.
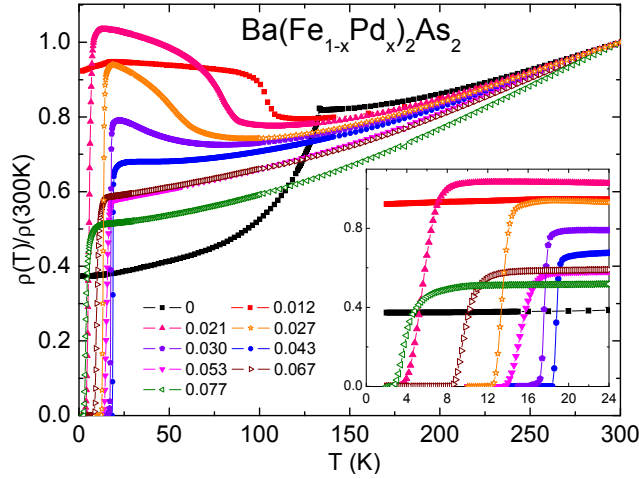

FIG. 4: The temperature dependent resistivity, normalized by room temperature value, for $Ba(Fe_{1-x}Pd_x)_2As_2$. Inset: low temperature data for $Ba(Fe_{1-x}Pd_x)_2As_2$

Fig. 4 shows the normalized electrical resistivity data for the $Ba(Fe_{1-x}Pd_x)_2As_2$ series from base temperature, 2 K, to 300 K. A systematic behavior, similar to the

Ba(Fe$_{1-x}$Rh$_x$)$_2$As$_2$ series, is seen: the temperature of the resistive anomaly associated with the structural / antiferromagnetic phase transitions is suppressed monotonically with Pd doping and the shape of the anomaly changes from a sharp decrease to a broadened increase in resistivity upon cooling. For $x = 0.021$, the resistive anomaly can still be clearly seen and superconductivity is detected with $T_c \approx 5.7$ K. For $x = 0.043$, the temperature of the resistive anomaly is further reduced and it is only inferred from a minimum in the resistivity above the superconducting transition. For $x = 0.053$, the resistive anomaly is completely suppressed and T_c has its highest value of about 19 K and a width of $\Delta T_c \approx 0.6$ K. With higher x values, T_c is suppressed.
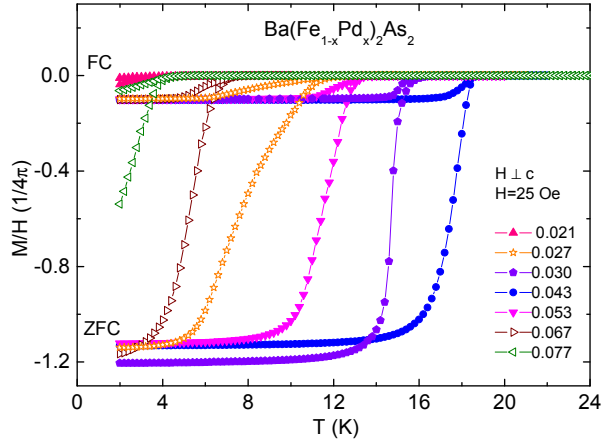

FIG. 5: Low magnetic field M/H for Ba(Fe$_{1-x}$Rh$_x$)$_2$As$_2$ series.

The low field M/H data for the Ba(Fe$_{1-x}$Pd$_x$)$_2$As$_2$ series (FC and ZFC) are shown in Fig. 5. They were taken at 25 Oe with H perpendicular to the crystallographic c-axis. The broader feature seen in the magnetization for $x = 0.027$ implies a larger inhomogeneity associated with this sample. Indeed, the WDS data for $x = 0.027$ does show local maximum in 2σ values. Despite the broader drop of the magnetization, the large superconducting fraction is comparable to the rest of the Pd- doped series as well as to the Co-, Ni- and Rh- doped BaFe$_2$As$_2$ results, all of which are consistent with bulk superconductivity. Again, only a small diamagnetic signal was observed at base temperature for $x = 0.021$ due to the low T_c for this concentration.

Fig. 6 shows the temperature dependent heat capacity data for Ba(Fe$_{0.957}$Pd$_{0.043}$)$_2$As$_2$, which manifests the highest T_c value in this series. The heat capacity anomaly at T_c can be clearly seen, although it is broader than the one found for Ba(Fe$_{0.943}$Rh$_{0.057}$)$_2$As$_2$ (Fig.

3). The arrows show the onset of superconductivity at $T_c = 18$ K, and the estimated $\triangle C_p$ is shown in the inset; $\triangle C_p \approx 410$ mJ/mole K. Using the BCS weak coupling approximation $\triangle C_p / \gamma T_c = 1.43$ and assuming 100% superconducting volume in this sample, γ for $Ba(Fe_{0.957}Pd_{0.043})_2As_2$ is estimated to be about 16 mJ/mole K^2.
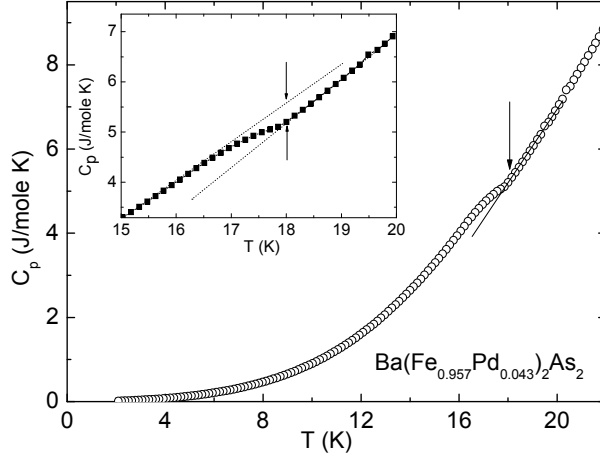

FIG. 6: Temperature dependent heat capacity data for $Ba(Fe_{0.957}Pd_{0.043})_2As_2$. Inset: C_p vs. T near the superconducting transition with the estimated $\triangle C_p$ shown.

IV. DISCUSSION

The data presented in Figs. 1 - 6 are summarized in the two, $T - x$, phase diagrams shown in Fig. 7. In this paper, the temperature of structrural/magnetic phase transitions are inferred from the derivative of the temperature dependent resistivity data which shows a split feature for finite values of x [11]. Onset and offset criteria, which are shown in the inset of Fig. 1, are used to determine T_c from the resistivity data. The criterion which is shown in the inset of Fig. 2 is used to determine T_c from the magnetization data. The arrows in Fig. 3 show the criterion used to infer T_c from heat capacity data. We can see good agreement between resistivity, magnetization and heat capacity measurements. So as to allow comparison with the isoelectronic, $3d$ electron doped $BaFe_2As_2$ compounds, data for $Ba(Fe_{1-x}TM_x)_2As_2$ (TM = Co, Ni) [11, 17] are also shown.

The upper panel presents the $T - x$ phase diagrams of Rh and Co doped $BaFe_2As_2$ and the lower panel presents the $T - x$ phase diagrams of Pd and Ni doped $BaFe_2As_2$. It can be seen in both panels that the higher temperature structural/magnetic phase transitions are
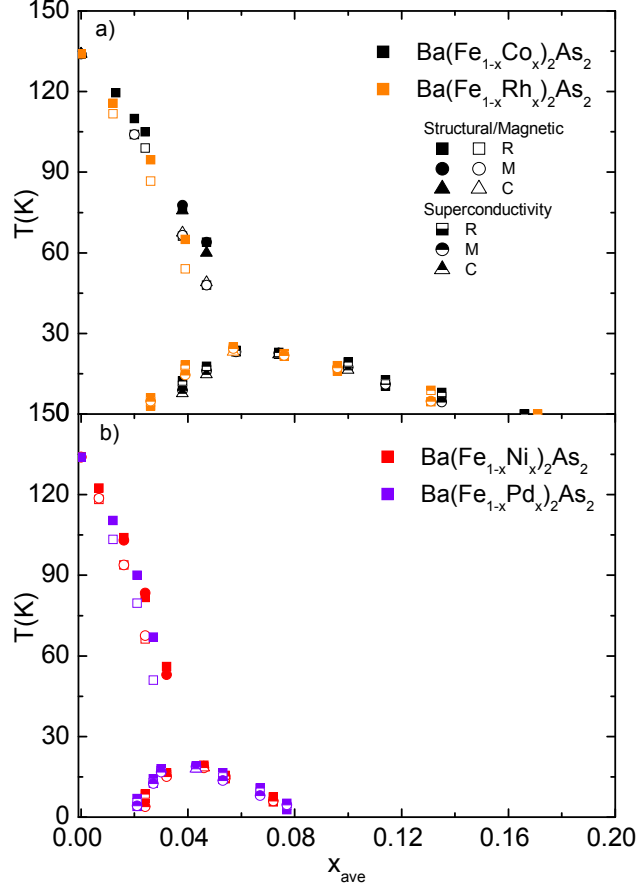
FIG. 7: Transition temperature as a function of x. (a): $T - x$ phase diagrams of Ba(Fe$_{1-x}$Rh$_x$)$_2$As$_2$ and Ba(Fe$_{1-x}$Co$_x$)$_2$As$_2$ series. (b): $T - x$ phase diagrams of Ba(Fe$_{1-x}$Pd$_x$)$_2$As$_2$ and Ba(Fe$_{1-x}$Ni$_x$)$_2$As$_2$ series. For both plots the transition temperatures were determined in a manner similar to that described in [11] and the text.

suppressed monotonically in a similar manner/rate for all series. Superconductivity is found in both tetragonal and orthorhombic phase [11, 12, 13, 14], and is stabilized in a dome-like region for all series. Superconductivity is found over a wider range of Co or Rh doping with a maximum T_c around 24 K, and a narrower range of Ni or Pd doping with a maximum T_c around 19 K.

The complete phase diagram of Rh doped BaFe$_2$As$_2$ including both structural/magnetic phase transition and superconductivity shows incredible similarity as the phase diagram of Co doped BaFe$_2$As$_2$ and the complete phase diagram of Pd doped BaFe$_2$As$_2$ shows incredible similarity as the phase diagram of Ni doped BaFe$_2$As$_2$. For each of the pairs, the

9

phase diagrams show exceptionally similar behavior on the rate of the suppression of structural/magnetic phase transitions, the range of superconducting domes and the maximum T_c. It is worth mentioning again that to see this, the actual x values are vital.
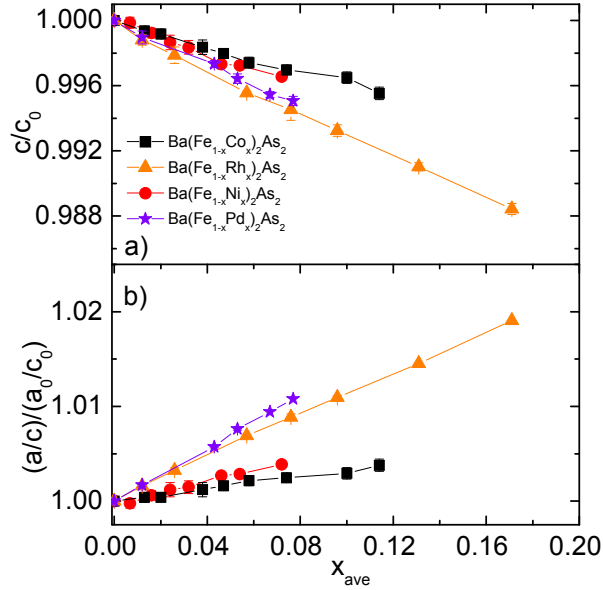

FIG. 8: Normalized structural parameters measured at ~ 300 K. (a) a/a_0, (b) $(a/c)/(a_0/c_0)$ as a function of transition metal doping, x. (a_0=3.9621(4) Å, c_0=13.0178(10) Å)

In our previous work [17], we compared the transition temperatures as a function of x, and as a function of the number of extra conduction electrons, e, added by the dopant per Fe/TM site for Co, Ni, Cu and Co/Cu doped BaFe$_2$As$_2$ (for the case of Co $e = x$, for the case of Ni $e = 2x$, for the case of Cu $e = 3x$). We conclude that whereas the suppression of the structural/antiferromagnetic transitions was parameterized by the number of TM dopant ions (or, equivalently, changes in the c-axis) the superconducting dome was parameterized by the number of electrons added by doping (or, equivalently, changes in the values of the a/c ratio), and exists over a limited range of e-values (or band filling). Unfortunately we could not experimentally separate the effects of x and e from changes in c and a/c, respectively [17]. However, with current, $4d$ electron doped BaFe$_2$As$_2$ data, we can actually distinguish between x and e on one hand and c, a/c on the other. Fig. 8 shows the unit cell parameters normalized by the lattice parameters of pure BaFe$_2$As$_2$. To compare the unit cell parameters, the data for Co or Ni doped BaFe$_2$As$_2$ [11, 17] are also plotted in Fig.8. The lattice parameter c decreases with all dopings and the ratio of a/c increases with all dopings.

But in both cases there is a clear difference between the 3d- and 4d- data sets. Unlike in our previous work [17], where for 3d electron doping series and c can be scaled with x, a/c can be scaled with the number of extra electron added per Fe/TM site, when 4d electron doped BaFe$_2$As$_2$ data are taken into account, changes in c and a/c are no longer equivalent to x and e. This means that if we want to parameterize the effects of 3d- and 4d-TM doping on the transitions temperatures of Ba(Fe$_{1-x}$TM$_x$)$_2$As$_2$, whereas the upper, structural and magnetic phase transitions can be parameterized by x and the superconducting dome can be parameterized by e, they are no longer well parameterized by either c or a/c. As discussed in [17], it is still possible that some other parameter, such as bonding angles associated with the As position, offer better or alternate parameterization of these transition temperatures, but these are not currently known.
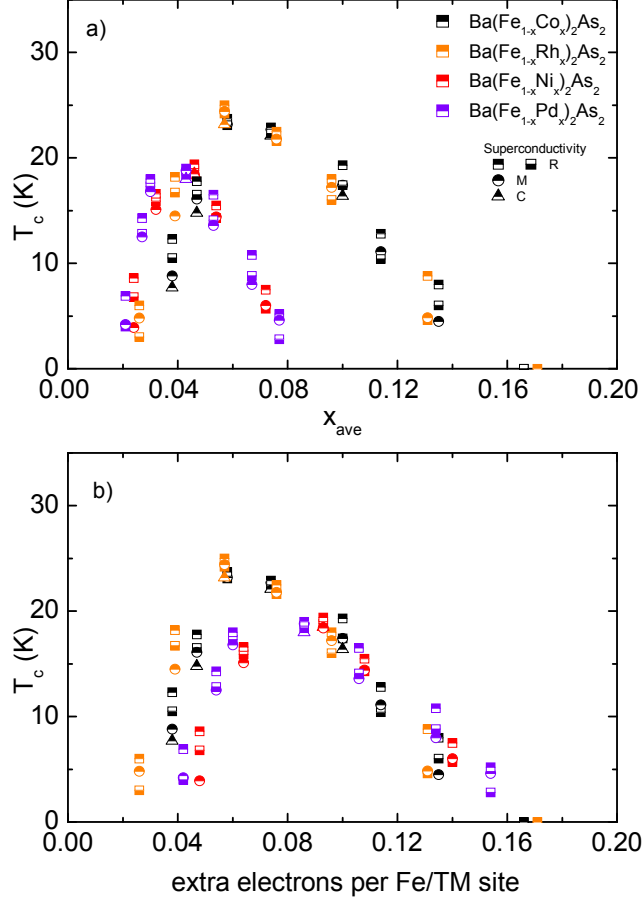

FIG. 9: (a): superconducting transition temperature T_c as a function of x_{ave}. (b): superconducting transition temperature T_c as a function of extra electrons per Fe/TM site.

The parameterization scheme outlined above is based on the premise that a single parameter may be controlling the variation of the upper, structural and magnetic transition temperatures ($T_{s/m}$) and a second one may be controlling the superconductivity. There is another scheme that should be discussed in the context of our growing data set: that there may be a single parameter that controls the behavior of the system when $T_{s/m} > T_c$ and there is another single parameter when $T_{s/m}$ is fully suppressed. The potential appeal of this scheme can be seen in Fig. 9, where T_c is plotted as a function of e and x for comparison. As discussed above and in reference [17], there is excellent agreement of the T_c values when plotted as a function of e when $T_{s/m}$ is fully suppressed. On the other hand there is arguably better agreement of the T_c values when they are plotted as a function of x for $T_{s/m} > T_c$. As pointed out in ref [17] the behavior on the $T_{s/m} > T_c$ side of the dome may be associated with the need to bring the upper transition to low enough temperature to allow the superconductivity to turn on. The importance of reducing $T_{s/m}$ may be associated with reducing the degree of orthorhombic splitting, the size of the ordered moment in the AF phase, and / or changing the magnetic excitation spectrum.

Given that $T_{s/m}$ only roughly scales with x it is worth while examining the correlation between T_s, T_m and T_c more directly. Fig. 10 plots T_c as a function of the structural, as well as the magnetic, transition temperature (given that they are split by the time superconductivity is stabilized) [11, 15, 16]. Both plots show a clear correlation. A more graphic way of examining the correlation between T_c and $T_{s/m}$ is to create a composite diagram for the $T_{s/m} > T_c$ data by adjusting the x scales for the Ni, Rh, and Pd data so as to collapse the T_s and T_m phase lines onto the Co data set. This is plotted in Fig. 11. As we can see, a clear consequence of this is to bring collapse the T_c data onto a single phase line as well.

V. CONCLUSION

Single crystalline $Ba(Fe_{1-x}TM_x)_2As_2$ (TM = Rh, Pd) samples have been grown and characterized by microscopic, thermodynamic and transport measurements. $T - x$ phase diagrams were constructed for both the Rh- and Pd-doping series and, remarkably, they are virtually indistinguishable from the $T - x$ phase diagrams assembled for their $3d$-shell counterpart, Co- and Ni-doped, series. Given that the variations of the unit cell parameters are distinctly different for the $3d$ and $4d$ dopants, these data clearly show that whereas the
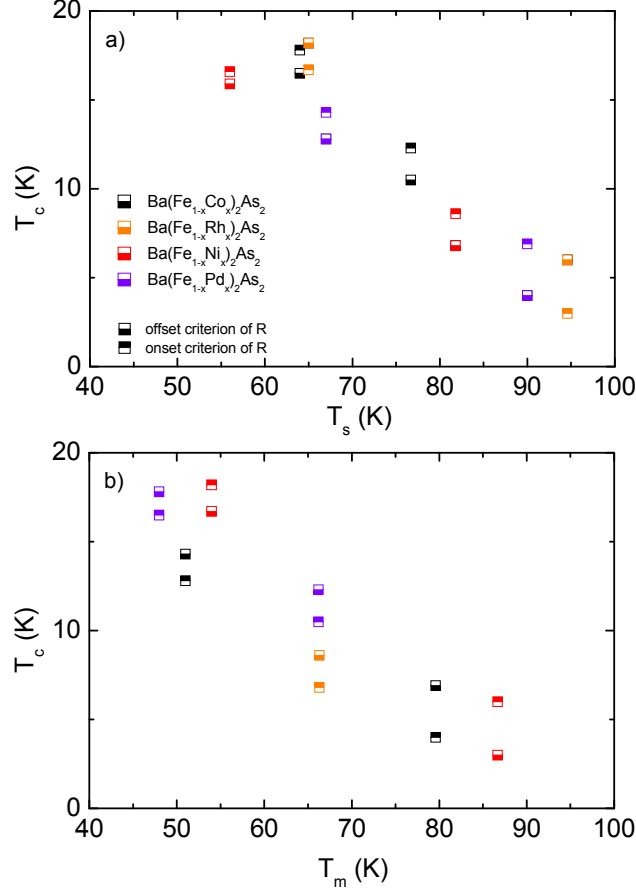
FIG. 10: (a): Superconducting transition temperature T_c as a function of structural phase transition temperature T_s. (b): Superconducting transition temperature T_c as a function of magnetic phase transition temperature T_m.

amount of dopant, x, and the change in electron count, e, do a fair job of parameterizing the structural / magnetic and superconducting phase transitions temperatures, respectively, the variation of the c-axis lattice parameter and the variation of the ratio of the a/c parameters no longer do.

Whereas the structural and magnetic phase transitions are fairly well parameterized by x and, for $T_c > T_{s/m}$, T_c is parameterized by e very well, the T_c data for $T_{s/m} > T_c$ appears to depend on the degree of suppression of $T_{s/m}$ (and therefore may depend more on x than on e). The fact that the behavior of T_c in response to doping appears to change in the vicinity of the disappearance of $T_{s/m}$ is consistent with recent studies of the $T - P$ phase diagram for $BaFe_2As_2$ [23] as well as earlier work on K-doped $BaFe_2As_2$ [24]. In every case
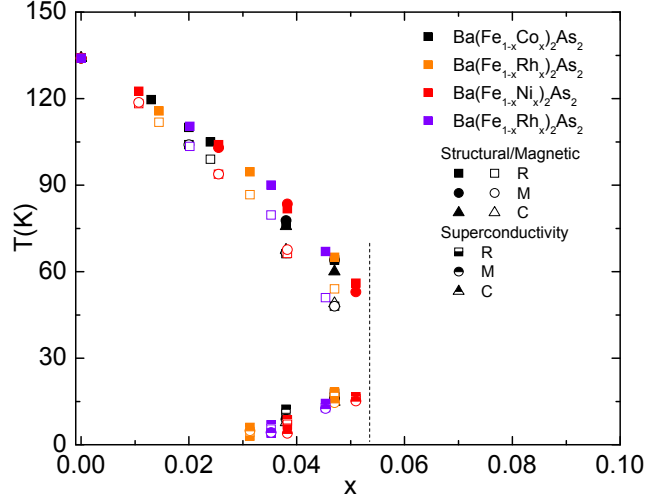
FIG. 11: Transition temperature as a function of adjusted x. x is normalized so as to bring the interpolated values of T_s onto the transition associated with $Ba(Fe_{0.953}Co_{0.047})_2As_2$: for Co doped $BaFe_2As_2$, $x = x_{ave}$; for Rh doped $BaFe_2As_2$, $x = x_{ave} \times 0.047/0.039$; for Pd doped $BaFe_2As_2$, $x = x_{ave} \times 0.047/0.028$; for Ni doped $BaFe_2As_2$, $x = x_{ave} \times 0.047/0.03$.

T_c appears to reach its maximum value (varying from TM-, to K-, to P-doped [25]) when $T_{s/m}$ is suppressed below T_c.

Acknowledgments

[1] Y. Kamihara, T. Watanabe, M. Hirano, and H. Hosono, J. Am. Chem. Soc. 130, 3296 (2008)

[2] M. Rotter, M. Tegel, and D. Johrendt , Phys. Rev. Lett. 101, 107006 (2008)

[3] Zhi-An Ren, Wei Lu, Jie Yang, Wei Yi, Xiao-Li Shen, Zheng-Cai Li, Guang-Can Che, Xiao-Li Dong, Li-Ling Sun, Fang Zhou, Zhong-Xian Zhao, Chin. Phys. Lett. 25, 2215 (2008)

[4] Athena S. Sefat, Rongying Jin, Michael A. McGuire, Brian C. Sales, David J. Singh, and David Mandrus, Phys. Rev. Lett. 101, 117004 (2008)

[5] L.J. Li, Y.K. Luo, Q.B. Wang, H. Chen, Z. Ren, Q. Tao, Y.K. Li, X. Lin, M. He, Z.W. Zhu, G.H. Cao and Z.A Xu , New Journal of Physics 11, 025008 (2009)

[6] Athena S. Sefat, Ashfia Huq, Michael A. McGuire, Rongying Jin, Brian C. Sales, David Mandrus, Lachlan M. D. Cranswick, Peter W. Stephens, and Kevin H. Stone, Phys. Rev. B 78, 104505 (2008)

[7] S. Paulraj, Shilpam Sharma, A. Bharathi, A. T. Satya, Sharat Chandra, Y. Hariharan, C. S. Sundar, unpublished, arXiv:0902.2728 (2009)

[8] Fei Han, Xiyu Zhu, Peng Cheng, Bing Shen, Hai-Hu Wen, unpublished, arXiv:0903.1028 (2009)

[9] Xiyu Zhu, Fei Han Peng Cheng, Bing Shen, Hai-Hu Wen, unpublished, arXiv:0903.0323 (2009)

[10] Fei Han, Xiyu Zhu, Ying Jia, Lei Fang, Peng Cheng, Huiqian Luo, Bing Shen, Hai-Hu Wen, unpublished, arXiv:0902.3957 (2009)

[11] N. Ni, M. E. Tillman, J.-Q. Yan, A. Kracher, S. T. Hannahs, S. L. Bud'ko, and P. C. Canfield, Phys. Rev. B 78, 214515 (2008)

[12] Jiun-Haw Chu, James G. Analytis, Chris Kucharczyk, and Ian R. Fisher, Phys. Rev. B 79, 014506 (2009)

[13] F.L. Ning, K. Ahilan, T. Imai, A. S. Sefat, R. Jin, M. A. McGuire, B. C. Sales, D. Mandrus, J. Phys. Soc. Jpn. 78, 013711 (2009)

[14] Lei Fang, Huiqian Luo, Peng Cheng, Zhaosheng Wang, Ying Jia, Gang Mu, Bing Shen, I. I. Mazin, Lei Shan, Cong Ren, Hai-Hu Wen, unpublished, arXiv:0903.2418 (2009)

[15] C. Lester, Jiun-Haw Chu, J. G. Analytis, S. Capelli, A. S. Erickson, C. L. Condron, M. F. Toney, I. R. Fisher, S.M. Hayden, Phys. Rev. B 79, 134528 (2009)

[16] D. K. Pratt, W. Tian, A. Kreyssig, J. L. Zarestky, S. Nandi, N. Ni, S. L. Bud'ko, P. C. Canfield, A. I. Goldman, R. J. McQueeney, unpublished, arXiv:0903.2833 (2009)

[17] P. C. Canfield, S. L. Bud'ko, N. Ni, J. Q. Yan, A. Kracher, unpublished, arXiv: 0904.3134 (2009)

[18] P. C. Canfield and Z. Fisk, Philos. Mag. B 65, 1117 (1992)

[19] M. A. Tanatar, N. Ni, C. Martin, R. T. Gordon, H. Kim, V. G. Kogan, G. D. Samolyuk, S. L. Budko, P. C. Canfield, and R. Prozorov, Phys. Rev. B 79, 094507 (2009)

[20] M. A. Tanatar, N. Ni, G. D. Samolyuk, S. L. Bud'ko, P. C. Canfield, R. Prozorov, Phys. Rev. B 79, 134528 (2009)

[21] Marianne Rotter, Marcus Tegel, Dirk Johrendt, Inga Schellenberg, Wilfried Hermes, and Rainer Pöttgen, Phys. Rev. B 78, 020503 (2008)

[22] S. L. Bud'ko, N. Ni, S. Nandi, G. M. Schmiedeshoff, and P. C. Canfield, Phys. Rev. B 79, 054525 (2009)

[23] E. Colombier, S. L. Bud'ko, N. Ni, P. C. Canfield, unpublished, arXiv:0904.4488 (2009)

[24] Rotter. Marianne, Pangerl. Michael, Tegel. Marcus, Johrendt. Dirk, Angew. Chem. Int. Ed. 47, 7949 (2008)

[25] Shuai Jiang, Cao Wang, Zhi Ren, Yongkang Luo, Guanghan Cao, Zhu'an Xu, unplublished, arXiv: 0901.3227 (2009)